Isoform-specific p73 knockout mice reveal a novel role for ΔNp73 in the DNA damage response pathway

Margareta T. Wilhelm,[1,2] Alessandro Rufini,[1,3] Monica K. Wetzel,[4,5] Katsuya Tsuchihara,[1,6] Satoshi Inoue,[1] Richard Tomasini,[1,7] Annick Itie-Youten,[1] Andrew Wakeham,[1] Marie Arsenian-Henriksson,[2] Gerry Melino,[3,8] David R. Kaplan,[4,9] Freda D. Miller,[5,9,10] and Tak W. Mak[1,11]

[1]The Campbell Family Institute for Breast Cancer Research, Princess Margaret Hospital, Toronto, Ontario M5G 2C1, Canada; [2]Department of Microbiology, Tumor and Cell Biology, Karolinska Institutet, 171 77 Stockholm, Sweden; [3]Toxicology Unit, Medical Research Council Leicester, Leicester LE1 9HN, United Kingdom; [4]Department of Cell Biology, Hospital for Sick Children, Toronto, Ontario M5G 1X8, Canada; [5]Department of Developmental and Stem Cell Biology, Hospital for Sick Children, Toronto, Ontario M5G 1X8, Canada; [6]Research Center for Innovative Oncology, National Cancer Center Hospital East, Kashiwa, Chiba 277-8577, Japan; [7]Institut National de la Sante et de la Recherche Medicale, Unite 624, Stress Cellulaire, Parc Scientifique et Technologique de Luminy, 13288 Marseille Cedex 9, France; [8]Biochemistry IDI-IRCCS Laboratory, c/o University of Rome "Tor Vergata," 00133 Rome, Italy; [9]Department of Molecular Genetics, University of Toronto, Toronto, Ontario M5G 1X5, Canada; [10]Department of Physiology, University of Toronto, Toronto, Ontario M5G 1X5, Canada

Mice with a complete deficiency of p73 have severe neurological and immunological defects due to the absence of all TAp73 and ΔNp73 isoforms. As part of our ongoing program to distinguish the biological functions of these isoforms, we generated mice that are selectively deficient for the ΔNp73 isoform. Mice lacking ΔNp73 (ΔNp73$^{-/-}$ mice) are viable and fertile but display signs of neurodegeneration. Cells from ΔNp73$^{-/-}$ mice are sensitized to DNA-damaging agents and show an increase in p53-dependent apoptosis. When analyzing the DNA damage response (DDR) in ΔNp73$^{-/-}$ cells, we discovered a completely new role for ΔNp73 in inhibiting the molecular signal emanating from a DNA break to the DDR pathway. We found that ΔNp73 localizes directly to the site of DNA damage, can interact with the DNA damage sensor protein 53BP1, and inhibits ATM activation and subsequent p53 phosphorylation. This novel finding may explain why human tumors with high levels of ΔNp73 expression show enhanced resistance to chemotherapy.

[*Keywords*: p73; p53; neurodegeneration; DNA damage response; apoptosis]

Supplemental material is available at http://www.genesdev.org.

Received October 12, 2009; revised version accepted January 27, 2010.

The DNA damage response (DDR) acts as an important barrier against tumorigenesis. This molecular pathway consists of a complex network of DNA damage sensors, signal transducers, and effectors. Among its central components are ATM, ATR, and DNA-PK, which are PI3K-related kinases whose substrates mediate cell cycle arrest, DNA repair, and apoptosis. ATM is recruited to DNA double-strand breaks (DSBs) by the Mre11–Rad50–Nbs1 (MRN) complex and thereby activated. Activated ATM amplifies the response by phosphorylating several target substrates, including the tumor suppressor p53. Upon phosphorylation by ATM, p53 is stabilized and activated, and induces cell cycle arrest and/or apoptosis (Banin et al. 1998; Canman et al. 1998). The gene encoding p53 (*TP53* in humans, *Trp53* in mice) is the most commonly mutated gene in adult human tumors (http://www.p53.iarc.fr; http://www.p53.free.fr). The importance of p53's tumor-suppressive role is reflected in *Trp53*-deficient mice (p53$^{-/-}$ mice), which rapidly develop tumors at high frequency (Donehower et al. 1992).

p53 is the prototypical member of a protein family that includes p63 and p73. These proteins share structural and functional homology, and act as transcription factors to regulate cellular proliferation, differentiation, and death (Melino et al. 2002). Although p53 family members transactivate an overlapping set of target genes, the generation of individual knockout (KO) mice has shown clearly that each family member regulates unique genetic programs. In contrast to p53 deficiency, disruption of the p63 gene (*Trp63*) results in severe developmental anomalies, whereas complete deletion of the p73 gene (*Trp73*) leads to neurological and immunological defects (Yang et al. 1999, 2000).

[11]Corresponding author.
E-MAIL tmak@uhnres.utoronto.ca; FAX (416) 204-5300.
Article published online ahead of print. Article and publication date are online at http://www.genesdev.org/cgi/doi/10.1101/gad.1873910.

The *Trp53*, *Trp63*, and *Trp73* genes each encode several different N-terminally truncated isoforms (ΔN) due to usage of an internal promoter. Additional isoforms result from alternative splicing of C-terminal exons (α–η) (Melino et al. 2002). Whereas full-length p53 family proteins such as p53, TAp73, and TAp63 function as transcription factors inducing cell cycle arrest, differentiation, or apoptosis, the ΔN isoforms block the transactivation activity of these molecules in a dominant-negative fashion (Grob et al. 2001). Thus, the ΔN isoforms act like oncogenes. The potential oncogenic effect of ΔNp73 is supported by several observations: (1) Overexpression of ΔNp73 facilitates cell immortalization and cooperates with oncogenic Ras^{V12} in cellular transformation (Stiewe et al. 2002); (2) cells overexpressing ΔNp73 promote tumor formation when injected into nude mice (Stiewe et al. 2002; Petrenko et al. 2003); and (3) Ras^{V12} is involved in biasing the TAp73/ΔNp73 ratio in favor of ΔNp73, and the resulting down-regulation of TAp73 and up-regulation of ΔNp73 are important for Ras transforming activity (Beitzinger et al. 2008).

The severe developmental defects exhibited by mice with a null mutation of *Trp73* (*Trp73*$^{-/-}$ or p73$^{-/-}$ mice) include hydrocephalus, hippocampal dysgenesis, and abnormalities of the pheromone sensory pathway. Furthermore, these mice succumb at an early age to chronic infections and inflammation (Yang et al. 2000). However, because these mutants lack both the TAp73 and ΔNp73 isoforms, it is difficult to assess the contribution of each isoform to the observed phenotypes. To shed light on this problem, we generated mice that are selectively deficient for either the TAp73 or ΔNp73 isoforms. We reported previously that mice lacking only the TAp73 isoforms (TAp73$^{-/-}$ mice) are infertile, show a high incidence of spontaneous tumors, and are very sensitive to chemical carcinogens (Tomasini et al. 2008, 2009). This work demonstrated that TAp73 is important for maintaining genomic stability, and established TAp73 as a bona fide tumor suppressor. In this study, we report the generation and characterization of mice lacking only the ΔNp73 isoforms (ΔNp73$^{-/-}$ mice). Unlike TAp73$^{-/-}$ mice, our ΔNp73$^{-/-}$ mice show signs of neurodegeneration, confirming previous reports describing a neuroprotective role for ΔNp73 (Pozniak et al. 2000; Tissir et al. 2009). More importantly, we demonstrate a novel role for ΔNp73 in inhibiting signal transduction from sites of DNA damage to the DDR pathway.

Results

Mice deficient for ΔNp73 are viable and fertile and have a normal life span, but display signs of neurodegeneration

We generated our ΔNp73$^{-/-}$ mice by specifically targeting exon 3′ of the *Trp73* gene (Supplemental Fig. 1A). This exon is expressed exclusively in ΔNp73 isoforms and not in TAp73 isoforms. The loss of ΔNp73 expression was confirmed at both the mRNA and protein levels (Supplemental Fig. 1B,C). No major differences were observed in TAp73 mRNA levels in the liver, testis, or lung of wild-type and ΔNp73$^{-/-}$ littermate mice (Supplemental Fig. 1D), demonstrating that our targeting strategy did not affect TAp73 isoforms. Mice deficient for ΔNp73 were born at the normal Mendelian ratio (wild type, 28%; heterozygote, 51%; KO, 20%), although we did note a slight, but significant (P = 0.0179), reduction in ΔNp73$^{-/-}$ females (wild type, 32%; heterozygote, 50%; KO, 18%) (Supplemental Fig. 1E). Both male and female ΔNp73$^{-/-}$ mice were fertile and enjoyed a normal life span (data not shown).

As stated above, p73$^{-/-}$ mice display severe neurological defects, including hippocampal dysgenesis, postnatal loss of neurons that results in greatly enlarged ventricles (hydrocephalus), and reduced cortical thickness (Yang et al. 2000). We showed previously that TAp73$^{-/-}$ mice display hippocampal dysgenesis similar to that in p73$^{-/-}$ mice, implying that TAp73 is essential for normal hippocampal development (Tomasini et al. 2008). However, ventricular size and cortical thickness were normal in TAp73$^{-/-}$ brains, suggesting that it is the loss of ΔNp73 in p73$^{-/-}$ mice that causes the abnormalities in these parameters. To test if ΔNp73$^{-/-}$ mice displayed CNS atrophy similar to that in p73$^{-/-}$ mice (Pozniak et al. 2002; Wetzel et al. 2008), we used Nissl staining to analyze the underlying cytoarchitecture of the motor cortex in wild-type and ΔNp73$^{-/-}$ mice at 10 mo and 26–27 mo of age. Measurement of coronal sections at equivalent rostrocaudal levels revealed that the width of the motor cortex from the corpus callosum to the pia (see the boxed region in Fig. 1A) did not differ between wild-type and ΔNp73$^{-/-}$ mice at 10 mo of age (Fig. 1B). However, neuronal density in the mutant was significantly reduced (61.61% of age-matched controls) (Fig. 1C,D). This decrease paralleled a concomitant increase in the number of condensed cells (127% of age-matched controls) (Fig. 1E). In contrast, by 26-27 mo of age, motor cortex thickness was reduced significantly in ΔNp73$^{-/-}$ mice (84.75% of controls) (Fig. 2A,B) and neuronal density was decreased significantly (61.38% of controls) (Fig. 2C,D). However, numbers of condensed cells in the motor cortex were not significantly different in wild-type and ΔNp73$^{-/-}$ mice at 26–27 mo (Fig. 2E). Taken together, these results indicate that ΔNp73$^{-/-}$ mice display neuroanatomical evidence of mild neurodegeneration.

ΔNp73$^{-/-}$ cells show enhanced expression of p53 target genes and increased apoptosis in response to DNA damage

It has been hypothesized that ΔNp73 might interfere with p53-mediated responses by competing with p53 for DNA-binding sites in target gene promoters (Zaika et al. 2002). Such binding would inhibit the expression of p53-induced genes such as p21, Mdm2, and Puma. To test this idea, we examined the expression of p53 target genes before and after DNA damage in primary mouse embryonic fibroblasts (MEFs) isolated from ΔNp73$^{-/-}$ embryos. Surprisingly, even in untreated ΔNp73$^{-/-}$ MEFs, we detected a modest increase in expression of p53 target genes

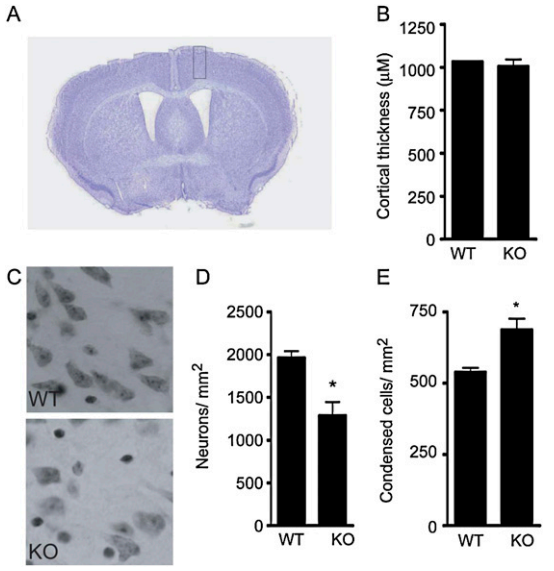

Figure 1. Loss of ΔNp73 reduces neuronal density in the brain. Brains from 10-mo-old wild-type (n = 5) and ΔNp73$^{-/-}$ (n = 4) mice were analyzed histologically. (*A*) Representative Nissl-stained coronal section of a 10-mo-old ΔNp73$^{-/-}$ mouse. Boxed region is the strip of cortical tissue spanning the corpus callosum to the pia that was assessed for cortical thickness. (*B*) Quantitation of cortical thickness. No differences in cortical thickness were detected between wild-type and ΔNp73$^{-/-}$ mice at 10 mo of age. (*C*,*D*) Reduced neuronal density. Cell density in the cortical strips of the mice in *A* and *B* was assessed histologically by Nissl staining (*C*) and was quantified (*D*) (ΔNp73$^{-/-}$, 1286 ± 160.6 neurons per square millimeter, vs. wild type, 1960 ± 79.98 neurons per square millimeter). Results in *D* are the mean ± SEM. (*E*) Increased frequency of condensed cells. Condensed cells in the cortical strips of the mice in *A* and *B* were counted (ΔNp73$^{-/-}$, 687.5 ± 38.45 condensed cells per square millimeter, vs. wild type, 538.6 ± 15.14 condensed cells per square millimeter). Results shown are the mean ± SEM.

compared with the wild type at both the mRNA and protein levels (Fig. 3A,B). These data indicate that, even in unstressed cells, ΔNp73 is required to dampen levels of p53 targets in order to avoid detrimental effects. Compared with unstressed wild-type MEFs, no increase in apoptosis was detected in unstressed ΔNp73$^{-/-}$ MEF cultures (data not shown). However, both MEFs and thymocytes from ΔNp73$^{-/-}$ mice showed heightened sensitivity to a wide range of DNA-damaging agents, including cisplatin, doxorubicin, etoposide, and γ-irradiation (Fig. 3C,D). These results suggest that lack of ΔNp73 sensitizes cells to the effects of DNA damage. Accordingly, in response to DNA damage, we observed a greater increase in mRNA expression of the proapoptotic p53 target PUMA in ΔNp73$^{-/-}$ MEFs than in controls (Fig. 3A). Importantly, the enhanced apoptotic response in thymocytes was reversed on a p53-null background (Fig. 3D), confirming that ΔNp73 is a negative regulator of p53-dependent apoptosis. Interestingly, we could not detect any difference between wild-type and ΔNp73$^{-/-}$ cells in response to UV treatment, TNFα treatment, or IL-2 withdrawal (data not shown), suggesting that ΔNp73 dampens the effects of certain types of apoptotic stress but not all.

Loss of ΔNp73 impairs tumor formation in vivo

To test whether ΔNp73 deficiency plays a role in tumor formation in vivo, we transformed primary MEFs from wild-type and ΔNp73$^{-/-}$ littermates with E1A and Ras^{V12} (Supplemental Fig. 2A). No differences were observed in proliferation rate in vitro or capacity to form colonies in soft agar (Supplemental Fig. 2B,C). However, when injected subcutaneously into athymic nude mice, transformed ΔNp73$^{-/-}$ MEFs formed tumors that were significantly smaller and at a slower rate than those arising in animals injected with wild-type MEFs (Fig. 4A,B), suggesting that loss of ΔNp73 impairs the ability of transformed cells to initiate new tumors. Surprisingly, this decrease in the size of tumors derived from ΔNp73$^{-/-}$ cells was not associated with an increase in apoptosis (data not shown). However, in agreement with recent reports on p53-mediated tumor suppressor activity in

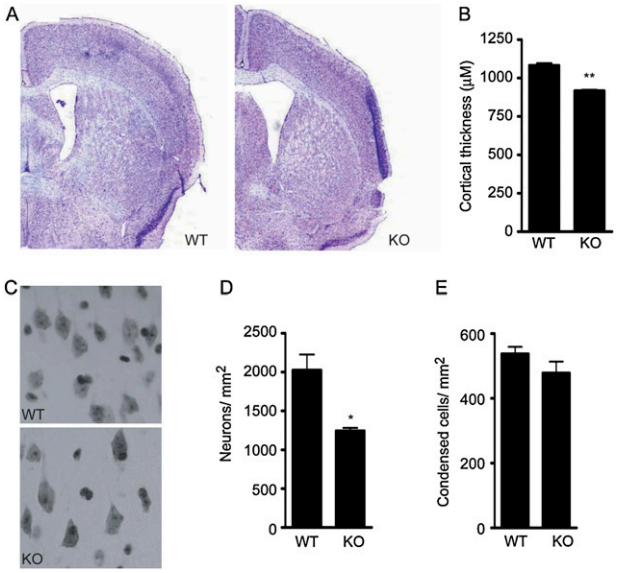

Figure 2. Aged ΔNp73$^{-/-}$ mice display signs of neurodegeneration. Brains from 26- to 27-mo-old wild-type (n = 2) and ΔNp73$^{-/-}$ (n = 2) mice were analyzed histologically. (*A*) Representative Nissl-stained coronal sections of 26- to 27-mo-old wild-type and ΔNp73$^{-/-}$ mice. A decrease in cortical thickness can be seen in the mutant compared with the wild type. (*B*) Quantitation of cortical thickness. A significant decrease in cortical thickness was detected in ΔNp73$^{-/-}$ mice at 26–27 mo of age compared with the wild type (ΔNp73$^{-/-}$, 917 ± 6.579 mm^2, vs. wild type, 1082 ± 14.12 mm^2). Results in *B* are the mean ± SEM. (*C*,*D*) Reduced neuronal density. Cell density in the cortical strips of the mice in *A* and *B* was assessed histologically by Nissl staining (*C*) and was quantified (*D*) (ΔNp73$^{-/-}$, 1243 ± 38.28 neurons per square millimeter, vs. wild type, 2025 ± 200 neurons per square millimeter). Results shown in *D* are the mean ± SEM. (*E*) Comparable frequency of condensed cells. Condensed cells in the cortical strips of the mice in *A* and *B* were counted, but no significant differences were observed.

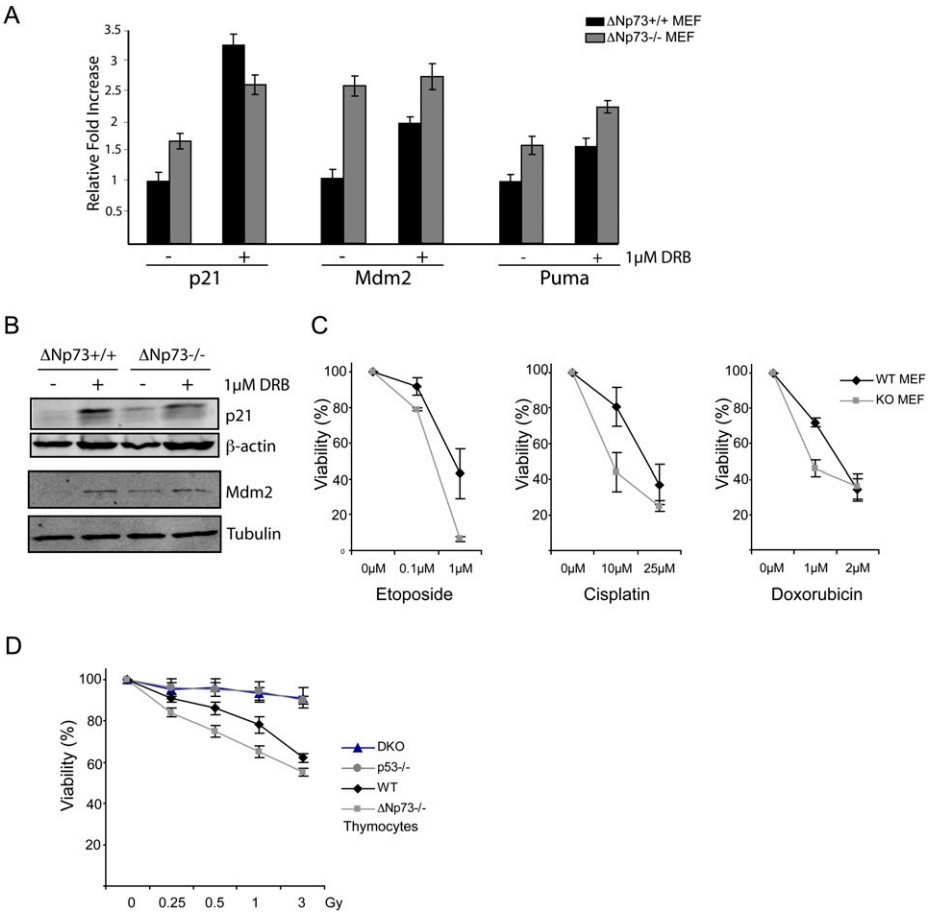

Figure 3. Loss of ΔNp73 increases expression of p53 target genes and enhances p53-mediated apoptosis. (*A*) Increased p53 target gene mRNA expression. Primary MEFs from wild-type or $\Delta Np73^{-/-}$ mice were left untreated or were treated with 1 μM doxorubicin (DRB) for 2 h, and mRNA expression levels of p21, Mdm2, and Puma were determined by quantitative PCR. Results shown are the fold increase relative to wild type. (*B*) Increased p53 target gene protein expression. Primary MEFs from wild-type or $\Delta Np73^{-/-}$ mice were left untreated or were treated with 1 μM DRB for 16 h, and protein levels of p21 and Mdm2 were determined by Western blotting. Actin and tubulin were used as loading controls. (*C*) Enhanced apoptosis. Wild-type and $\Delta Np73^{-/-}$ MEFs were treated with the indicated concentrations of the indicated apoptosis-inducing agents for 24 h. Cell viability was determined by Annexin V/PI staining and flow cytometry. (*D*) p53 dependence of enhanced apoptosis. Thymocytes from wild-type, $\Delta Np73^{-/-}$, $p53^{-/-}$, or $p53^{-/-}\Delta Np73^{-/-}$ double-KO (DKO) mice were subjected to the indicated doses of γ-irradiation, and apoptosis was determined 16 h later as for *C*.

vivo (Ventura et al. 2007; Xue et al. 2007), we did detect an increase in ΔNp73-deficient tumors of the senescence markers senescence-associated β-galactosidase (SA-β-gal), $p16^{INK4A}$, and DcR2 (Fig. 4C,D). The p53 target gene DcR2 has been identified as a marker for oncogene-induced senescence and is found expressed in premalignant tumors, but expression is lost upon transition to malignant tumors (Collado et al. 2005; Liu et al. 2005). Our results therefore suggest that ΔNp73 is needed for transformed cells to establish tumors in vivo, possibly by inhibiting senescence.

ΔNp73 inhibits the phosphorylation and activation of ATM and p53 induced by DNA damage

The dominant-negative effect of ΔNp73 on the transactivation abilities of p53 and TAp73 is thought to stem from competition for binding to the same DNA sequences in target gene promoters (Grob et al. 2001). However, we detected higher levels of p53 protein in $\Delta Np73^{-/-}$ MEFs treated with either cisplatin or doxorubicin than in wild-type MEFs treated with these agents (Fig. 5A,B; Supplemental Fig. 3A). These results suggest that the observed increase in DNA damage-induced apoptosis in $\Delta Np73^{-/-}$ cells may be due not only to a lack of competition for binding to target gene promoters, but also to increased p53 activity. The ATM protein is rapidly activated in response to DNA damage, and is one of the kinases responsible for phosphorylation of Ser15 of human p53 (Ser18 of murine p53) (Banin et al. 1998; Canman et al. 1998). Phosphorylation of p53Ser15 leads to a concomitant phosphorylation of its N-terminal Thr18, Ser9, and Ser20 residues that in turn abrogates p53:Mdm2 interaction and inhibits 26S proteosome-mediated degradation of p53 (Saito et al. 2003). DNA damage also triggers the autophosphorylation of ATM at Ser1981 (Ser1987 in

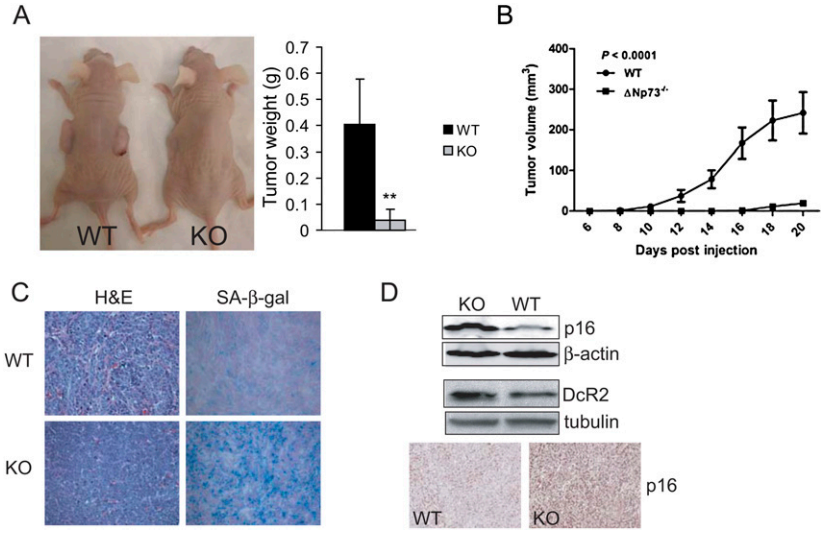

Figure 4. Loss of ΔNp73 impairs tumor formation in nude mice. (*A*) Decreased tumor formation. E1A/Ras^{V12}-transformed wild-type or ΔNp73$^{-/-}$ MEFs were injected subcutaneously into both flanks of athymic Balb/c nu/nu mice (n = 8 per group). The ability to form tumors was assessed at 2 wk post-injection. (*Left* panel) Gross presentation of representative nude mice injected with either wild-type or ΔNp73$^{-/-}$ MEFs. (*Right* panel) Histogram showing the average weight of tumors derived in the nu/nu mice from wild-type and ΔNp73$^{-/-}$ transformed MEFs (wild type, n = 15; ΔNp73$^{-/-}$, n = 11). Tumors derived from ΔNp73$^{-/-}$ cells were found to be significantly smaller than those derived from wild-type cells (ΔNp73$^{-/-}$, 0.04 g ± 0.016 g, vs. wild type, 0.4 g ± 0.14 g). Results shown are the mean ± SD. P = 0.008. (*B*) Tumor kinetics. E1A/Ras^{V12}-transformed wild-type or ΔNp73$^{-/-}$ MEFs were injected subcutaneously into either flank of athymic Balb/c nu/nu mice (n = 13). Tumor mass was assessed at 2-d intervals up to 20-d post-injection. Tumors derived from ΔNp73$^{-/-}$ cells grow at a significantly slower rate than those derived from wild-type cells. Results are shown as the mean ± SEM. $P < 0.0001$. (*C*,*D*) Increased expression of senescence markers. Tumors derived from ΔNp73$^{-/-}$ cells show increase in SA-β-gal (*C*), p16^{INK4A}, and DcR2 (*D*) compared with wild-type cells. Results are representative of four tumors from each genotype.

murine ATM). Although work in mouse models has shown that this residue is dispensable for ATM function, its phosphorylation correlates with DSB-induced activation of ATM, and thus is still useful as a marker of ATM kinase activity (Pellegrini et al. 2006; Daniel et al. 2008). We examined our wild-type and ΔNp73$^{-/-}$ MEFs after exposure to DNA damage and detected higher amounts of phosphorylated p53Ser18 in the mutant cells (Fig. 5B,C), indicating that deletion of ΔNp73 leads to increased activation of p53.

We next investigated the activation of ATM by doxorubicin or γ-irradiation in ΔNp73$^{-/-}$ cells and tissues. We detected increased phosphorylation of ATMSer1987 in ΔNp73$^{-/-}$ MEFs, thymocytes, and skin tissue subjected to DNA damage (Fig. 5C–E), as well as increased phosphorylation (activation) of the ATM substrate histone H2AX (Fig. 5E). To further elucidate the role of ATM in the increased apoptotic sensitivity of ΔNp73$^{-/-}$ cells, we crossed ΔNp73$^{-/-}$ mice with ATM$^{-/-}$ mice and subjected thymocytes from the doubly deficient offspring to γ-irradiation. Irradiated ΔNp73$^{-/-}$ATM$^{-/-}$ thymocytes show similar resistance to apoptosis as ATM$^{-/-}$ thymocytes (Fig. 5F), suggesting that, along with p53, ATM is required for the enhanced apoptosis observed in ΔNp73$^{-/-}$ cells.

We next tested if the above results could be recapitulated in human tumor cells by using siRNA to knock down ΔNp73 expression in U2OS cells (osteosarcoma cells expressing wild-type p53) (Supplemental Fig. 4A). Notably, ΔNp73 knockdown strongly sensitized U2OS cells to DNA damage-induced cell death (Fig. 6A). Moreover, phosphorylation of ATMSer1981 and ATM/ATR substrates (Fig. 6B), as well as expression of p53, PUMA, and p21 (Supplemental Fig. 4B,C), were increased when ΔNp73 was depleted. To investigate the significance of p53 in these events, we employed isogenic strains of the human colon cancer cell line HCT116 that are wild type or deficient for p53 (HCT116$^{p53+/+}$ or HCT116$^{p53-/-}$). Significantly, the ability of ΔNp73 knockdown to sensitize HCT116$^{p53+/+}$ cells to DNA damage was impaired by p53 deletion (Supplemental Fig. 4D). To confirm the inhibitory effects of ΔNp73 on p53-mediated responses to DNA damage, we ectopically overexpressed the ΔNp73β isoform in U2OS cells. Upon γ-irradiation, we observed decreased ATM phosphorylation, reduced p53 protein accumulation, and decreased PUMA protein expression in the presence of excessive ΔNp73β (Fig. 6C,D). Thus, our data suggest that ΔNp73 interferes with the DDR pathway and impairs ATM and p53 activation.

ΔNp73 interacts with 53BP1 and localizes to sites of DNA damage

We next sought to investigate how ΔNp73 influences the activation of ATM and p53 in response to DNA damage. No differences in total ATM mRNA or protein levels was detected in ΔNp73$^{-/-}$ cells compared with wild-type cells after DNA damage, and no direct binding between ΔNp73 and ATM could be demonstrated (data not shown). It has been shown previously that the complete activation of ATM and p53 depends on their interaction with 53BP1 (Zgheib et al. 2005). Mice deficient for 53BP1 show enhanced tumor formation and decreased radiosensitivity, similar to mice deficient for p53 (Ward et al. 2003). Crystal structure analysis has revealed that 53BP1 and p53 interact through the DNA-binding domain of p53 (Derbyshire et al. 2002). Importantly, several residues critical for 53BP1–p53 interaction are conserved in ΔNp73 (Supplemental Fig. 5A). Consequently, we tested whether ΔNp73 was able to bind to 53BP1. We transfected U2OS cells with HA-tagged ΔNp73α or ΔNp73β,

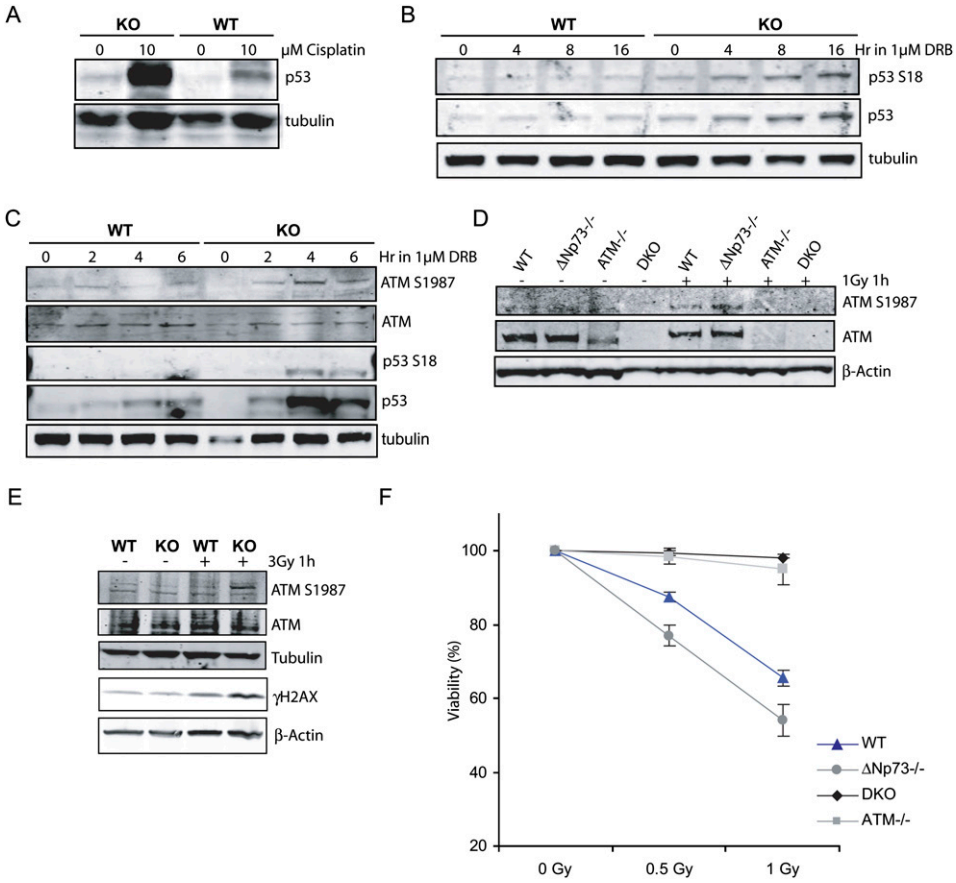

Figure 5. Increased p53 and ATM phosphorylation and activation in ΔNp73-deficient cells and tissues upon DNA damage. (*A*) Increased p53 protein levels. Wild-type and $\Delta Np73^{-/-}$ MEFs were treated with 10 μM cisplatin for 16 h, and p53 protein was analyzed by Western blot. (*B,C*) Increased p53Ser18 and ATMSer1987 phosphorylation. Wild-type and $\Delta Np73^{-/-}$ MEFs were treated with 1 μM DRB for a long (*B*) or short (*C*) time course as indicated, and total and phosphorylated p53 and ATM were analyzed by Western blot. (*D*) Increased ATMSer1987 phosphorylation in thymocytes. Wild-type and $\Delta Np73^{-/-}$ thymocytes were γ-irradiated as indicated, and total and phosphorylated ATM levels were assessed by Western blot. (*E*) Increased ATMSer1987 phosphorylation and γ-H2AX induction in skin tissue. Skin tissue from wild-type and $\Delta Np73^{-/-}$ mice were γ-irradiated as indicated, and total ATM, phosphorylated ATM, and γ-H2AX protein levels were assessed by Western blot. (*F*) The increased sensitivity to DNA damage in $\Delta Np73^{-/-}$ thymocytes is ATM-dependent. Thymocytes from mice of the indicated genotypes were γ-irradiated as indicated, and apoptosis was determined 16 h later by Annexin V/PI staining and flow cytometry. DKO, $\Delta Np73^{-/-}ATM^{-/-}$ mice.

immunoprecipitated endogenous 53BP1, and detected direct binding of 53BP1 to ΔNp73β, but not to ΔNp73α, both before and after DNA damage (Fig. 7A). We could also observe binding with reverse immunoprecipitation when ectopically expressing 53BP1 and Flag-tagged ΔNp73β in U2OS cells (Supplemental Fig. 5B). To confirm that this interaction occurred at physiological levels of ΔNp73, we examined the binding between endogenous 53BP1 and endogenous ΔNp73. We therefore took advantage of a recently developed ΔNp73-specific antibody that can detect endogenous ΔNp73 (Sayan et al. 2005). We subjected extracts of neuroblastoma SH-SY5Y cells to immunoprecipitation with 53BP1 antibody followed by Western blotting using anti-ΔNp73 antibody and confirmed that 53BP1 can bind to endogenous ΔNp73β but not to ΔNp73α (Fig. 7B). Interestingly, the binding between 53BP1 and ΔNp73 was unaffected by DNA damage when the ΔNp73 protein was ectopically expressed, but was lost in irradiated cells with physiological levels of ΔNp73. The reduced binding between 53BP1 and ΔNp73β in the latter case is probably due to a reduction in levels of ΔNp73β protein present after DNA damage. Indeed, it has been reported previously that ΔNp73 is degraded upon DNA damage to allow for apoptosis (Maisse et al. 2004). In any case, we confirmed that binding occurred between ΔNp73β and 53BP1 in U2OS cells using the in situ proximity ligation assay (PLA), which allows detection of protein interaction in situ. Although a weak binding between ΔNp73 and 53BP1 occurred in untreated cells, this interaction was greatly enhanced in γ-irradiated cells (Fig. 7C).

To determine whether ΔNp73 could localize directly to sites of DNA damage, we used H2AX as a marker of DNA damage foci. Upon DNA damage, residue Ser139 of H2AX is phosphorylated by ATM within minutes, resulting in γ-H2AX. γ-H2AX then forms foci at DSB sites. In U2OS cells ectopically expressing ΔNp73, we could not detect

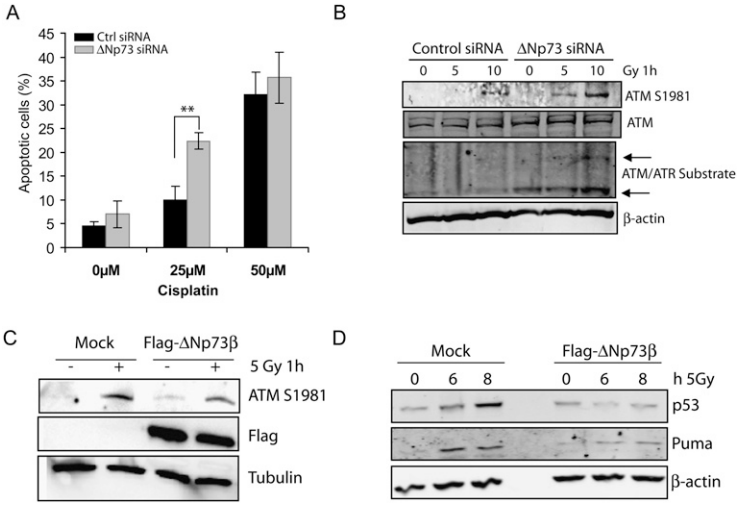

Figure 6. ΔNp73 interferes with ATM and p53 activation in human tumor cells. (*A*) Sensitization to apoptosis in the absence of ΔNp73. Human osteosarcoma U2OS cells were treated with control siRNA (black bars) or siRNA against ΔNp73 (gray bars) for 24 h, and then exposed for an additional 24 h to the indicated doses of cisplatin. Apoptosis was determined by Annexin V/PI staining and flow cytometry. (*B*) Increased ATM activation in the absence of ΔNp73. U2OS cells were treated with control siRNA or siRNA against ΔNp73 for 48 h, and phosphorylation levels of ATMSer1981 and ATM/ATR substrates were determined at 1 h after exposure to the indicated levels of γ-irradiation by Western blotting. (*C*,*D*) Overexpression of ΔNp73β impairs ATMSer1981 phosphorylation, p53 protein accumulation, and Puma expression. U2OS cells engineered to ectopically express ΔNp73β or a mock vector were exposed to 5 Gy γ-irradiation for the indicated times, and protein levels of phospho-ATMSer1987 (*C*), or p53 and Puma (*D*) were determined by Western blotting.

localization of the overexpressed ΔNp73 protein to DNA damage foci (data not shown). However, when we examined the colocalization of endogeous p73 and γ-H2AX in doxorubicin-treated H1299 nonsmall lung carcinoma cells, we found that these two proteins colocalized at DSB sites (Fig. 7D). This could also be recapitulated with endogenous ΔNp73 and γ-H2AX in irradiated SH-SY5Y cells within 10 min of γ-irradiation (Fig. 7E). These results indicate that ΔNp73 localizes to sites of DNA damage under physiological conditions.

Finally, to examine the effect of ΔNp73 depletion on the assembly of DNA damage foci, we used siRNA to knock down ΔNp73 expression in U2OS cells and analyzed focus formation in response to γ-irradiation. Indeed, depletion of ΔNp73 enhanced the degree of recruitment of 53BP1, p53, and γ-H2AX to DSB sites (Fig. 7F; Supplemental Fig. 5C). These results show that endogenous ΔNp73 interacts with 53BP1 and localizes to sites of DNA damage, where ΔNp73 decreases the recruitment of DDR proteins to this site. ΔNp73 is thus a negative regulator of the DDR, consistent with the observation that ΔNp73 dysregulation promotes oncogenesis.

Discussion

Disruption of *Trp73* results in profound neurological defects, but the relative contributions of the TAp73 and ΔNp73 isoforms to this phenotype have not been investigated thoroughly due to a lack of isofom-specific mouse models. We addressed this problem by generating mice specifically deficient for TAp73 or ΔNp73. We reported previously that TAp73$^{-/-}$ mice showed hippocampal dysgenesis similar to that in *Trp73*-null mice, thus defining a role for TAp73 in the development of the CNS (Tomasini et al. 2008). With our present generation of mice specifically deficient for ΔNp73, and our observation of the neurodegeneration that occurs in these mutants as they age, we confirmed a neuroprotective function for the ΔNp73 isoform. This was also observed in a recent study by Tissir et al. (2009) that also constructed ΔNp73-null mice. In their mouse model, they noted that vomeronasal neurons and Cajal-Rezius cells were severely reduced in number, and that choroid plexuses were atrophic (Tissir et al. 2009). It should be noted, however, that the severity of the neurological defects observed in the isoform-specific mouse models is not as dramatic as that reported for p73$^{-/-}$ mice, suggesting that TAp73 and ΔNp73 may partially overlap in their functions. Furthermore, there are phenotypes observed in p73$^{-/-}$ mice that are not recapitulated in either of the isoform-specific mouse models, such as the severe chronic infections and inflammation that eventually kill p73$^{-/-}$ mice. This discrepancy suggests that either isoform can fully compensate for the loss of the other in these latter biological processes. To fully resolve the functions of all p73 isoforms, mouse models bearing C-terminal-specific disruptions of *Trp73* should be generated.

Several reports have indicated that ΔNp73 acts downstream from p53 as a transcriptional negative regulator that competes for binding motifs in target promoters (Grob et al. 2001; Zaika et al. 2002). Our results are consistent with this hypothesis, since our ΔNp73-deficient MEFs exhibit increased levels of p21, Mdm2, and Puma under resting conditions. Interestingly, in response to DNA damage, higher mRNA levels of Mdm2 and Puma but not p21 were induced in ΔNp73$^{-/-}$ MEFs compared with the wild type. This observation suggests that the loss of ΔNp73 makes some target promoters more accessible, thus directing the cell toward a particular biological outcome. In line with this theory, we observed an elevation in sensitivity to apoptotic stimuli in cells lacking ΔNp73. This increased sensitivity was lost in cells with a p53-null background, proving that ΔNp73 does indeed inhibit p53-dependent apoptosis.

A particularly interesting finding emerging from our study is that, compared with wild-type controls, no increase in apoptosis was detected in tumors developing from E1A/Ras^{V12} transformed ΔNp73$^{-/-}$ MEFs, even though loss of ΔNp73 greatly inhibits tumor-forming

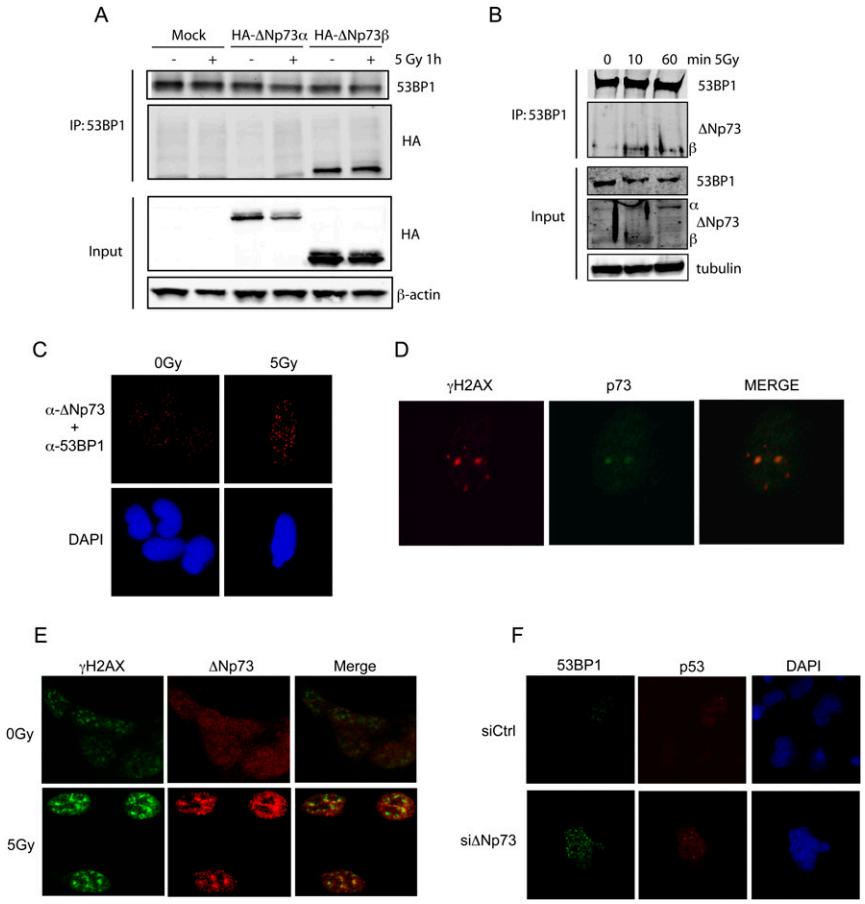

Figure 7. ΔNp73 interacts with 53BP1 and localizes to sites of DNA damage. (*A*) Overexpressed ΔNp73β, but not ΔNp73α, binds to 53BP1. U2OS cells were transiently transfected 24 h with constructs expressing HA-tagged ΔNp73α or ΔNp73β, and then were left untreated or were treated for 1 h with 5 Gy γ-irradiation. Cell extracts were immunoprecipitated with anti-53BP1 antibody to detect the binding of each ΔNp73 isoform to endogenous 53BP1. (*B*) Endogenous ΔNp73 binds to endogenous 53BP1. SH-SY5Y neuroblastoma cells were left untreated or were treated with 5 Gy γ-irradiation for the indicated times. Extracts were immunoprecipitated with anti-*53BP1* and subjected to Western blotting. The copurification of ΔNp73 and 53BP1 decreases after γ-irradiation. (*C*) PLA confirming that an interaction between 53BP1 and ΔNp73β occurs in response to DNA damage. U2OS cells grown on coverslips were transfected with a plasmid expressing ΔNp73β. After 24 h, transfected cells were left untreated or were subjected to 5 Gy γ-irradiation, incubated for 10 min, and fixed and stained to detect 53BP1:ΔNp73 interaction. Red dots in the confocal microscopic images indicate positivity for 53BP1:ΔNp73 interaction. Nuclei were stained with DAPI. (*D*) Detection of endogenous p73 in DNA damage foci. H1299 cells were grown on coverslips, treated with 2 μM doxorubicin, and fixed after 10 min. Cells were stained with anti-p73 antibody (green) and with antibody to detect the DNA damage focus marker γ-H2AX (red). Merged fluorescence shows that p73 colocalizes with γ-H2AX and DNA damage foci upon DNA damage. (*E*) Detection of endogenous ΔNp73 in DNA damage foci. SH-SY5Y cells were grown on coverslips, treated with 5 Gy γ-irradiation, and fixed after 10 min. Cells were stained with anti-ΔNp73 antibody (red) and with antibody to detect the DNA damage focus marker γ-H2AX (green). Merged fluorescence shows that ΔNp73 colocalizes with γ-H2AX and DNA damage foci upon γ-irradiation. (*F*) siRNA knockdown confirmation of ΔNp73 colocalization with DNA damage foci. U2OS cells expressing either control siRNA or siRNA against ΔNp73 were cultured for 48 h. Cells were then either left untreated or treated with 5 Gy γ-irradiation, fixed after 10 min, and immunostained to detect 53BP1 and p53. Confocal microscopy shows that depletion of ΔNp73 increases the recruitment and colocalization of 53BP1 (green) and p53 (red) to sites of DNA damage.

capacity in vivo. Instead, we observed an increase in senescence markers in tumor cells lacking ΔNp73. This phenomenon has also been reported in mouse models where p53 was restored in murine liver carcinomas or sarcomas (Ventura et al. 2007; Xue et al. 2007). While restoration of p53 in these established tumors induced cellular senescence and tumor regression, restoration of p53 in lymphomas resulted in apoptosis. This body of evidence suggests that, not unexpectedly, the biological outcome of p53 activation is very much dependent on cellular context. Interestingly, we detected increased levels of the tumor suppressor $p16^{INK4A}$, suggesting an involvement of the $p16^{INK4}$–RB pathway in the senescence phenotype triggered by loss of ΔNp73. Indeed, activation of the $p16^{INK4A}$–RB axes is known to play a role in the establishment of senescence in tumors and to act in parallel to or overlapping with the Arf–p53 axes (Campisi and d'Adda di Fagagna 2007; Collado and Serrano 2010). Notably, it has been shown that N-terminal-truncated isoforms of p73 inactivate RB by increased phosphorylation, thus triggering E2F activity and consequent cell proliferation (Stiewe et al. 2003). Intriguingly, our data might unveil a p53-independent function of ΔNp73 in regulating tumor growth. Further investigations are needed to clarify and extend these findings.

We were surprised to detect not only higher levels of p53 target gene expression in $\Delta Np73^{-/-}$ cells exposed to DNA damage, but also higher levels of the p53 protein itself. Because of the pivotal role p53 plays in controlling the cell cycle and cell death, this protein is tightly regulated at the transcriptional, translational, and post-translational levels (Fu et al. 1996; Ashcroft et al. 1999; Webster and Perkins 1999). However, the most important way by which p53 protein levels are controlled is through Mdm2-mediated degradation. In response to DNA damage, p53 is stabilized via phosphorylation of N-terminal residues (Ser15 and Ser20 in humans; Ser18 and Ser23 in mice). This phosphorylation interferes with Mdm2 binding to p53 and

prevents the proteasomal degradation of p53. To study the importance of p53Ser18 phosphorylation in p53-mediated responses, mouse models in which p53Ser18 is mutated have been created. Using such a model, Sluss et al. (2004) showed that phosphorylation of p53Ser18 is required for apoptosis and the induction of Puma that occur in response to DNA damage, but not for DNA damage-induced cell cycle arrest. Similarly, we found that an increase in p53Ser18 phosphorylation occurred in ΔNp73$^{-/-}$ cells following DNA damage, and that this increase was associated with enhanced apoptosis but not cell cycle arrest. Sluss et al. (2004) initially reported that, unlike p53-null mice, p53Ser18Ala mutants did not show accelerated tumorigenesis. However, re-examination of these mutants has revealed that they do, in fact, develop spontaneous tumors (predominantly B-cell lymphomas), but at a more advanced age than p53-null mice. Moreover, some of these p53Ser18Ala animals manifested symptoms of accelerated aging. Taken together, these data indicate that the ATM/ATR phosphorylation site Ser18 in p53 contributes to tumor suppression and organismal longevity (Armata et al. 2007), and perturbation of this pathway through elevated levels of ΔNp73 could contribute to tumor development.

Another intriguiging observation coming out of our study was that we detected binding only between 53BP1 and ΔNp73β and not between 53BP1 and ΔNp73α. The reason for this could be due to structural differences between ΔNp73β and ΔNp73α proteins, since p73α proteins (TAp73α and ΔNp73α) contain a sterile α motif (SAM) domain in their extreme C-terminal. It is thought that the SAM domain prevents binding of p300/CBP to TAp73α, thus inhibiting the transcriptional activity of TAp73α (Liu and Chen 2005). It is possible that the SAM domain in ΔNp73α also inhibits the binding of 53BP1 to ΔNp73α as well.

The integrity of the DNA damage checkpoints is a crucial barrier against tumor development. Analysis of precancerous lesions (before p53 mutations are acquired) repeatedly reveals signs of an activated DDR, including 53BP1 focus formation and phosphorylation of ATM, Chk2, and p53 (Bartkova et al. 2005; Gorgoulis et al. 2005). Once these lesions progress to malignancy, the evidence of DNA damage still exists, but mutations in components of the DDR pathway abolish the checkpoint response (Halazonetis et al. 2008). Our results suggest that the ΔNp73 isoform has a heretofore unsuspected role in the signaling pathway running from DSBs to the DDR pathway, and inhibits full activation of ATM and p53, possibly through its binding to 53BP1. Supporting ΔNp73's potential function as an oncogene, elevated levels of ΔNp73 have been found in neuroblastomas and medulloblastomas, as well as in lung, liver, ovarian, and cervical cancers. Moreover, increased ΔNp73 expression in tumors has been correlated with chemotherapeutic failure and poor patient survival (Casciano et al. 2002; Uramoto et al. 2004; Concin et al. 2005; Muller et al. 2005; Liu et al. 2006; Zitterbart et al. 2007). Our finding that ΔNp73 is a negative regulator of the DDR may explain why tumors with high levels of ΔNp73 show increased resistance to chemotherapy; thus, targeting ΔNp73 could be an effective weapon against several types of malignancies.

Materials and methods

Generation of ΔNp73$^{-/-}$ mice

Mutant mice deficient for *Trp73* exon 3′, which is specific for ΔNp73 isoforms, were generated by conventional gene targeting procedures in Sv129/Ola embryonic stem (ES) cells. Four correctly targeted ES cell clones were selected for blastocyst injection. Blastocysts were transferred to pseudopregnant C57BL/6J female mice to generate chimaeric mice. We obtained germline transmission of the targeted allele for all four ES cell clones. Littermate offspring that were wild type or heterozygous or homozygous for the mutated ΔNp73 allele were created by intercrossing ΔNp73$^{+/-}$ mice. Genotypes were confirmed by PCR analysis. The wild-type and KO ΔNp73 alleles were detected using the following primer pairs: wild-type sense, 5′-CAATTAG CAGCCTGGTCTCTGCCTGAC-3′; wild-type antisense, 5′-GG TAGGCTGGAGAGTGGACAGGTTC-3′; KO sense, 5′-GCTTCA TGGAGATAACTTCGTATAGCAT-3′; KO antisense, 5′-GGTAGG CTGGAGAGTGGACAGGTTC-3′. Experiments were conducted using mice from all four ΔNp73 mouse strains, and on both the mixed background (F1 intercross, 129/B6) and the backcrossed C57BL/6J background (F5), with equal results. The p53$^{-/-}$ and ATM$^{-/-}$ mice were on C57BL/6J background. All animals were treated in accordance with the NIH Guide for Care and Use of Laboratory Animals as approved by the Ontario Cancer Institute Animal Care Committee.

Neuroanatomy

For histology, 10-mo-old mice (n = 4–5 per group) and 26- to 27-mo-old mice (n = 2 per group) were sacrificed by sodium pentobarbital overdose (Somnitol, MTC) and transcardially perfused with PBS followed by 4% paraformaldehyde. Tissues were cryoprotected and sectioned at 16 μm, and Nissl staining was performed as described (Pozniak et al. 2002). Neuroanatomical parameters were measured in the motor cortex at the same rostrocaudal level, and were quantified in a strip of cortical tissue 325 μm wide that extended from the corpus callosum to the pial surface, as shown in Figure 2B. Cell density was calculated using the area of this strip and cell counts (Pozniak et al. 2002). All digital image acquisition was performed using a Sony XC-75CE CCD video camera equipped with Northern Eclipse software (Empix, Inc.). Image processing was carried out using ImageJ analysis software (National Institutes of Health).

Cell lines

MEFs were prepared from embryonic day 13.5 (E13.5) wild-type and ΔNp73$^{-/-}$ littermate embryos and cultured in Dulbecco's modified Eagle's medium (DMEM) supplemented with 10% fetal bovine serum (FBS), 2 mM L-glutamine, and 55 μM β-mercaptoethanol. Cells at passages 2–4 were used for experiments. The same medium was used to maintain human tumor cells (U2OS osteosarcoma, SH-SY5Y neuroblastoma, and H1299 nonsmall lung carcinoma were from American Type Culture Collection; HCT116 [p53$^{+/+}$ and p53$^{-/-}$] colon carcinoma cells were kindly provided by Dr. Bert Vogelstein, Johns Hopkins Oncology Center).

Real-time PCR

Total RNA was prepared using Trizol (Invitrogen) and treated with RNase-free DNase (Promega). Total RNA (1 μg) was used for cDNA synthesis using SuperScript III according to the manufacturer's instructions (Invitrogen). Real-time PCR using SYBR green dye was carried out on an ABI 7700 (Applied Biosystems) according to the manufacturer's instructions. Samples were run in triplicate and normalized to 18S RNA or GAPDH. Relative expression was calculated using the $\Delta\Delta C_T$ method.

Western blotting

Protein extracts were prepared using NP-40 buffer (50 mM Tris-HCl at pH 8, 120 mM NaCl, 1% NP-40, protease inhibitor cocktail [Roche], phosphatase inhibitor [Roche]). Total protein (50 μg) was fractionated by SDS-PAGE. High-molecular-weight proteins (ATM and 53BP1) were separated using 3%–8% Tris-acetate gels (Invitrogen). Fractionated proteins were transferred to PVDF membranes (Millipore) using standard transfer techniques, or to nitrocellulose membranes using the iBlot system (Invitrogen). Blots were incubated with antibodies recognizing the following proteins: p53 (FL393 and DO1; 1:1000), HA-probe (1:1000), and p16 (F12; 1:250) from Santa Cruz Biotechnologies; p21 (SXM30; 1:200), 53BP1 (mAb; 1:1000), and p53 (pAb240; 1:500) from BD Biosciences; Puma, phospho-p53Ser15, 53BP1 (Rb Ab), and phospho-ATM/ATR substrate (all used at 1:1000) from Cell Signaling Technology; phospho-ATM S1981 (1:500) from Rockland; ATM (2C1; 1:200)) from GeneTex, Inc.); γ-H2AX (1:1000) from Upstate Biotechnologies; DcR2 (1:200) from GeneTex, Inc.; and ΔNp73-specific antibody (Rb Ab; 1:1000). Bands were visualized and quantified using the Odyssey Infrared Imaging System (LI-COR Bioscience).

Tumor formation in vivo

MEFs were transduced with the E1A and Ras^{V12} oncogenes using retroviral infection (pLPC-E1A-IRES-Ras^{V12}) and selected by growth in puromycin (1 μg/mL) for 1–2 wk. Cells were considered transformed based on morphology and ability to form colonies in soft agar. Transformed cells (1×10^6) were injected subcutaneously into the flanks of 5-wk-old athymic Balb-c nu/nu male mice (n = 8 per group) (Taconic). Tumor growth was assessed at 2 wk post-injection. Tumor kinetics was obtained using the same conditions as above, except mice were injected with both genotypes (wild-type cells into left flank and KO cells into right flank). Tumor mass was measured every second day up to 20 d post-injection when the experiment was terminated, and tumors were harvested and processed for histology (for protocols, see the Supplemental Material).

Apoptosis

To quantify the apoptosis of thymocytes in vitro, thymocytes were isolated from 8- to 12-wk-old male mice, irradiated with 0.25–3 Gy γ-irradiation, and assayed after 16 h. For MEFs, the cells were plated overnight in six-well plates (1×10^5 cells per well) and treated the following day with cisplatin, doxorubicin, or etoposide (all from Sigma-Aldrich) (at the concentrations indicated in the figures). For human tumor cells, the cells were plated in six-well plates at 50% confluency and transfected with siRNA against human ΔNp73 or a control siRNA (Santa Cruz Biotechnologies) using Lipofectamin2000 according to the manufacturer's instructions. Apoptotic cells were detected by Annexin V/propidium iodide (PI) staining (BD Biosciences) and flow cytometry.

Immunoprecipitation

To assess binding between 53BP1 and ΔNp73, U2OS cells (1×10^6) were transfected with pcDNA (control), pcDNA-HA-ΔNp73α, or pcDNA-HA-ΔNp73β using Lipofectamine2000 according to the manufacturer's instructions. Cells were lysed in Chaps buffer (40 mM HEPES at pH 7.5, 120 mM NaCl, 1 mM EDTA, 10 mM Na-pyrophosphate, 10 mM β-glycerophosphate, 50 mM NaF, 1 mM $NaVO_3$, 0.3% Chaps, protease inhibitor cocktail [Roche]) and precleared with protein G sepharose beads (Amersham). Immunoprecipitation was carried out using 500 μg of precleared protein lysate plus 1 μg of anti-53BP1 antibody (Rb). To confirm reverse binding, pEGFPc1-53BP1 was transfected into U2OS cells stably expressing Flag-ΔNp73b, and cells were lysed in Chaps buffer. Immunoprecipitation was carried out using 500 μg of precleared protein lysate plus 1 μg of anti-Flag (M2, Sigma-Aldrich) covalently bound to protein G sepharose beads (Amersham). To assess the binding of endogenous 53BP1 and ΔNp73 proteins, SH-SY5Y cells (1×10^7) were treated with 5 Gy γ-irradiation and incubated for 10 or 60 min. Proteins were cross-linked for 10 min with 15 μM DSP (Dithiobis [succinimidyl propionate]; Pierce), lysed in Chaps buffer, and briefly sonicated. Protein extract (1 mg) was precleared with beads as above, and 1 μg of anti-53BP1 (BD Bioscience) was used for immunoprecipitation. Immunocomplexes were collected with protein G sepharose beads, washed in Chaps buffer, and boiled in 2× SDS sample buffer prior to Western blotting.

Immunofluorescence

Cells were grown directly on glass coverslips for 24 h before indicated treatment. Cells were then fixed and permeabilized with 2% paraformaldehyde–0.2% Triton X-100 for 10 min at room temperature, and further permeabilized by 20 min incubation in PBS–0.5% NP40. After 1 h of blocking in PBS–5% normal goat serum, cells were incubated overnight with the following antibodies: anti-phospho-H2AX (Upstate Biotechnologies), ΔNp73-specific antibody (Sayan et al. 2005), anti-53BP1 (BD Bioscience), and anti-p53 (Santa Cruz Biotechnologies). All antibodies were diluted in blocking solution 1:100. After extensive washing in PBS, cells were incubated for 1 h at room temperature with fluorophore-conjugated secondary antibodies (1:1000; Invitrogen). Nuclei were detected by DAPI staining. Images were acquired and analyzed using a Zeiss LSM510 confocal microscope.

We also used the Duolink in situ PLA from Olink Bioscience to detect interactions between 53BP1 and ΔNp73. Briefly, U2OS cells were transfected with a plasmid encoding ΔNp73 and plated 24 h later on glass coverslips. At 48 h post-transfection, the cells were fixed as described above. The fixed cells were incubated with the following primary antibodies: mouse mAb against p73 (Neomarker Ab4) and rabbit pAb against 53BP1 (Cell Signaling). The Duolink system provides oligonucleotide-labeled secondary antibodies (PLA probes) to each of the primary antibodies that, in combination with a DNA amplification-based reporter system, generate a signal only when the two primary antibodies are in close proximity. The signal from each detected pair of primary antibodies was visualized as a spot (please see the manufacturer's instructions for more details).

Statistical analysis

Apoptosis data and tumor weight were analyzed by Student's t-test, data are presented as mean ± SD, and P-values <0.05 were considered statistically significant. Tumor kinetics were analyzed by two-way ANOVA using GraphPad Prism, and presented

as mean ± SEM. *P*-values for offspring distribution were calculated by χ^2 using GraphPad Prism.

Acknowledgments

We gratefully acknowledge C. Gorrini for technical advice and helpful discussions, and M.E. Saunders for scientific editing. This work was supported by grants from the Canadian Institute of Health Research, Åke Wiberg foundation (M.T.W), and O.E. and Edla Johansson foundation (M.T.W). M.T.W., A.R., M.K.W., K.T., S.I., R.T., A.I., and A.W. conducted research for the paper. M.T.W., A.R., and T.W.M., wrote the paper. We all discussed the results and read the paper.

References

Armata HL, Garlick DS, Sluss HK. 2007. The ataxia telangiectasia-mutated target site Ser18 is required for p53-mediated tumor suppression. *Cancer Res* **67:** 11696–11703.

Ashcroft M, Kubbutat MH, Vousden KH. 1999. Regulation of p53 function and stability by phosphorylation. *Mol Cell Biol* **19:** 1751–1758.

Banin S, Moyal L, Shieh S, Taya Y, Anderson CW, Chessa L, Smorodinsky NI, Prives C, Reiss Y, Shiloh Y, et al. 1998. Enhanced phosphorylation of p53 by ATM in response to DNA damage. *Science* **281:** 1674–1677.

Bartkova J, Horejsi Z, Koed K, Kramer A, Tort F, Zieger K, Guldberg P, Sehested M, Nesland JM, Lukas C, et al. 2005. DNA damage response as a candidate anti-cancer barrier in early human tumorigenesis. *Nature* **434:** 864–870.

Beitzinger M, Hofmann L, Oswald C, Beinoraviciute-Kellner R, Sauer M, Griesmann H, Bretz AC, Burek C, Rosenwald A, Stiewe T. 2008. p73 poses a barrier to malignant transformation by limiting anchorage-independent growth. *EMBO J* **27:** 792–803.

Campisi J, d'Adda di Fagagna F. 2007. Cellular senescence: When bad things happen to good cells. *Nat Rev Mol Cell Biol* **8:** 729–740.

Canman CE, Lim DS, Cimprich KA, Taya Y, Tamai K, Sakaguchi K, Appella E, Kastan MB, Siliciano JD. 1998. Activation of the ATM kinase by ionizing radiation and phosphorylation of p53. *Science* **281:** 1677–1679.

Casciano I, Mazzocco K, Boni L, Pagnan G, Banelli B, Allemanni G, Ponzoni M, Tonini GP, Romani M. 2002. Expression of ΔNp73 is a molecular marker for adverse outcome in neuroblastoma patients. *Cell Death Differ* **9:** 246–251.

Collado M, Serrano M. 2010. Senescence in tumours: Evidence from mice and humans. *Nat Rev Cancer* **10:** 51–57.

Collado M, Gil J, Efeyan A, Guerra C, Schuhmacher AJ, Barradas M, Benguria A, Zaballos A, Flores JM, Barbacid M, et al. 2005. Tumour biology: Senescence in premalignant tumours. *Nature* **436:** 642.

Concin N, Hofstetter G, Berger A, Gehmacher A, Reimer D, Watrowski R, Tong D, Schuster E, Hefler L, Heim K, et al. 2005. Clinical relevance of dominant-negative p73 isoforms for responsiveness to chemotherapy and survival in ovarian cancer: Evidence for a crucial p53–p73 cross-talk in vivo. *Clin Cancer Res* **11:** 8372–8383.

Daniel JA, Pellegrini M, Lee JH, Paull TT, Feigenbaum L, Nussenzweig A. 2008. Multiple autophosphorylation sites are dispensable for murine ATM activation in vivo. *J Cell Biol* **183:** 777–783.

Derbyshire DJ, Basu BP, Serpell LC, Joo WS, Date T, Iwabuchi K, Doherty AJ. 2002. Crystal structure of human 53BP1 BRCT domains bound to p53 tumour suppressor. *EMBO J* **21:** 3863–3872.

Donehower LA, Harvey M, Slagle BL, McArthur MJ, Montgomery CA Jr, Butel JS, Bradley A. 1992. Mice deficient for p53 are developmentally normal but susceptible to spontaneous tumours. *Nature* **356:** 215–221.

Fu L, Minden MD, Benchimol S. 1996. Translational regulation of human p53 gene expression. *EMBO J* **15:** 4392–4401.

Gorgoulis VG, Vassiliou LV, Karakaidos P, Zacharatos P, Kotsinas A, Liloglou T, Venere M, Ditullio RA Jr, Kastrinakis NG, Levy B, et al. 2005. Activation of the DNA damage checkpoint and genomic instability in human precancerous lesions. *Nature* **434:** 907–913.

Grob TJ, Novak U, Maisse C, Barcaroli D, Luthi AU, Pirnia F, Hugli B, Graber HU, De Laurenzi V, Fey MF, et al. 2001. Human ΔNp73 regulates a dominant negative feedback loop for TAp73 and p53. *Cell Death Differ* **8:** 1213–1223.

Halazonetis TD, Gorgoulis VG, Bartek J. 2008. An oncogene-induced DNA damage model for cancer development. *Science* **319:** 1352–1355.

Liu G, Chen X. 2005. The C-terminal sterile α motif and the extreme C terminus regulate the transcriptional activity of the α isoform of p73. *J Biol Chem* **280:** 20111–20119.

Liu X, Yue P, Khuri FR, Sun SY. 2005. Decoy receptor 2 (DcR2) is a p53 target gene and regulates chemosensitivity. *Cancer Res* **65:** 9169–9175.

Liu SS, Chan KY, Cheung AN, Liao XY, Leung TW, Ngan HY. 2006. Expression of ΔNp73 and TAp73α independently associated with radiosensitivities and prognoses in cervical squamous cell carcinoma. *Clin Cancer Res* **12:** 3922–3927.

Maisse C, Munarriz E, Barcaroli D, Melino G, De Laurenzi V. 2004. DNA damage induces the rapid and selective degradation of the ΔNp73 isoform, allowing apoptosis to occur. *Cell Death Differ* **11:** 685–687.

Melino G, De Laurenzi V, Vousden KH. 2002. p73: Friend or foe in tumorigenesis. *Nat Rev Cancer* **2:** 605–615.

Muller M, Schilling T, Sayan AE, Kairat A, Lorenz K, Schulze-Bergkamen H, Oren M, Koch A, Tannapfel A, Stremmel W, et al. 2005. TAp73/Δ Np73 influences apoptotic response, chemosensitivity and prognosis in hepatocellular carcinoma. *Cell Death Differ* **12:** 1564–1577.

Pellegrini M, Celeste A, Difilippantonio S, Guo R, Wang W, Feigenbaum L, Nussenzweig A. 2006. Autophosphorylation at serine 1987 is dispensable for murine Atm activation in vivo. *Nature* **443:** 222–225.

Petrenko O, Zaika A, Moll UM. 2003. ΔNp73 facilitates cell immortalization and cooperates with oncogenic Ras in cellular transformation in vivo. *Mol Cell Biol* **23:** 5540–5555.

Pozniak CD, Radinovic S, Yang A, McKeon F, Kaplan DR, Miller FD. 2000. An anti-apoptotic role for the p53 family member, p73, during developmental neuron death. *Science* **289:** 304–306.

Pozniak CD, Barnabe-Heider F, Rymar VV, Lee AF, Sadikot AF, Miller FD. 2002. p73 is required for survival and maintenance of CNS neurons. *J Neurosci* **22:** 9800–9809.

Saito S, Yamaguchi H, Higashimoto Y, Chao C, Xu Y, Fornace AJ Jr, Appella E, Anderson CW. 2003. Phosphorylation site interdependence of human p53 post-translational modifications in response to stress. *J Biol Chem* **278:** 37536–37544.

Sayan AE, Paradisi A, Vojtesek B, Knight RA, Melino G, Candi E. 2005. New antibodies recognizing p73: Comparison with commercial antibodies. *Biochem Biophys Res Commun* **330:** 186–193.

Sluss HK, Armata H, Gallant J, Jones SN. 2004. Phosphorylation of serine 18 regulates distinct p53 functions in mice. *Mol Cell Biol* **24:** 976–984.

Stiewe T, Zimmermann S, Frilling A, Esche H, Putzer BM. 2002. Transactivation-deficient ΔTA-p73 acts as an oncogene. *Cancer Res* **62:** 3598–3602.

Stiewe T, Stanelle J, Theseling CC, Pollmeier B, Beitzinger M, Putzer BM. 2003. Inactivation of retinoblastoma (RB) tumor suppressor by oncogenic isoforms of the p53 family member p73. *J Biol Chem* **278:** 14230–14236.

Tissir F, Ravni A, Achouri Y, Riethmacher D, Meyer G, Goffinet AM. 2009. ΔNp73 regulates neuronal survival in vivo. *Proc Natl Acad Sci* **106:** 16871–16876.

Tomasini R, Tsuchihara K, Wilhelm M, Fujitani M, Rufini A, Cheung CC, Khan F, Itie-Youten A, Wakeham A, Tsao MS, et al. 2008. TAp73 knockout shows genomic instability with infertility and tumor suppressor functions. *Genes & Dev* **22:** 2677–2691.

Tomasini R, Tsuchihara K, Tsuda C, Lau SK, Wilhelm M, Ruffini A, Tsao MS, Iovanna JL, Jurisicova A, Melino G, et al. 2009. TAp73 regulates the spindle assembly checkpoint by modulating BubR1 activity. *Proc Natl Acad Sci* **106:** 797–802.

Uramoto H, Sugio K, Oyama T, Nakata S, Ono K, Morita M, Funa K, Yasumoto K. 2004. Expression of ΔNp73 predicts poor prognosis in lung cancer. *Clin Cancer Res* **10:** 6905–6911.

Ventura A, Kirsch DG, McLaughlin ME, Tuveson DA, Grimm J, Lintault L, Newman J, Reczek EE, Weissleder R, Jacks T. 2007. Restoration of p53 function leads to tumour regression in vivo. *Nature* **445:** 661–665.

Ward IM, Minn K, van Deursen J, Chen J. 2003. p53 Binding protein 53BP1 is required for DNA damage responses and tumor suppression in mice. *Mol Cell Biol* **23:** 2556–2563.

Webster GA, Perkins ND. 1999. Transcriptional cross talk between NF-κB and p53. *Mol Cell Biol* **19:** 3485–3495.

Wetzel MK, Naska S, Laliberte CL, Rymar VV, Fujitani M, Biernaskie JA, Cole CJ, Lerch JP, Spring S, Wang SH, et al. 2008. p73 regulates neurodegeneration and phospho-tau accumulation during aging and Alzheimer's disease. *Neuron* **59:** 708–721.

Xue W, Zender L, Miething C, Dickins RA, Hernando E, Krizhanovsky V, Cordon-Cardo C, Lowe SW. 2007. Senescence and tumour clearance is triggered by p53 restoration in murine liver carcinomas. *Nature* **445:** 656–660.

Yang A, Schweitzer R, Sun D, Kaghad M, Walker N, Bronson RT, Tabin C, Sharpe A, Caput D, Crum C, et al. 1999. p63 is essential for regenerative proliferation in limb, craniofacial and epithelial development. *Nature* **398:** 714–718.

Yang A, Walker N, Bronson R, Kaghad M, Oosterwegel M, Bonnin J, Vagner C, Bonnet H, Dikkes P, Sharpe A, et al. 2000. p73-deficient mice have neurological, pheromonal and inflammatory defects but lack spontaneous tumours. *Nature* **404:** 99–103.

Zaika AI, Slade N, Erster SH, Sansome C, Joseph TW, Pearl M, Chalas E, Moll UM. 2002. ΔNp73, a dominant-negative inhibitor of wild-type p53 and TAp73, is up-regulated in human tumors. *J Exp Med* **196:** 765–780.

Zgheib O, Huyen Y, DiTullio RA Jr, Snyder A, Venere M, Stavridi ES, Halazonetis TD. 2005. ATM signaling and 53BP1. *Radiother Oncol* **76:** 119–122.

Zitterbart K, Zavrelova I, Kadlecova J, Spesna R, Kratochvilova A, Pavelka Z, Sterba J. 2007. p73 expression in medulloblastoma: TAp73/ΔNp73 transcript detection and possible association of p73α/ΔNp73 immunoreactivity with survival. *Acta Neuropathol* **114:** 641–650.